Structural Efficiency Of Stitched Rod-Stiffened Composite Panels With Stiffener Crippling

Dawn C. Jegley*
NASA Langley Research Center, Hampton, Virginia 23681

and

Alexander Velicki** and Daniel A. Hansen+
The Boeing Company, Huntington Beach, California 92647

The structural efficiency of rod-stiffened stitched specimens is evaluated to determine their weight saving potential if the stiffeners were allowed to buckle at less than or equal to design ultimate load. Analytical and experimental results from rod-stiffened and blade-stiffened single-stiffener specimens are presented. In both cases, skin and flanges were stitched together through-the-thickness prior to curing. No mechanical fasteners were used for the assembly. Specimens were loaded to failure in axial compression. Failure modes are discussed. Finite element and experimental results agree for the response of the structures. For some specimen configurations, improved structural efficiency can be obtained by allowing stiffeners to buckle at design limit load rather than requiring that buckling not occur prior to design ultimate load. In addition, through-the-thickness stitching can change the failure mechanism by suppressing delamination between skin and flange. A parametric study is presented herein which describes the possible weight savings with this approach.

I. Introduction

NASA, Boeing and the Air Force Research Laboratory (AFRL) have been involved in the development of technologies needed for future low-cost, light-weight composite structures for transport aircraft for many years. As part of the NASA-Boeing effort, a stitched graphite-epoxy material system was developed with the potential for reducing the weight and cost of transport aircraft load-bearing structure.[1] By stitching through the thickness of a dry graphite-epoxy material system, the labor associated with panel fabrication and assembly can be significantly reduced. By stitching through the thickness to join elements such as pre-stacked skin segments, stringers, intercostals, ribs, and spar caps, the need for mechanical fasteners is almost eliminated and the stitching provides a mechanism to reduce damage growth resulting from events such as low-speed or discrete-source impact.

Conventional composites use a no-damage-growth approach and are sized such that discrete-source-damaged structure can support design limit load without damage propagation and barely visible impact-damaged structure can support design ultimate load without damage propagation. Meeting this restriction implies lower strain allowables than would be needed in a pristine structure, thereby leading to thicker structure and increased weight. Stitching arrests damage and allows the composite structure to meet aircraft damage requirements the same way as aluminum structure does.[1] This fail-safe damage arrestment approach (instead of a no-damage-growth approach) results in a higher strain allowable and lower weight. By reducing the effects of impact damage, the structure can be loaded to operate with large deformations which correspond to higher allowable strains. When this feature is included in the design process, the structural efficiency can be improved compared to structures designed with a no-damage-growth approach.

Structural efficiency is expressed in terms of weight versus load carrying capability.[2,3] Traditionally, the maximum load capacity for a structure was identified as the lowest of the loads corresponding to either allowable stress or strain or the minimum buckling load. For structural panels with adhesively bonded stringers, the primary reason for the buckling restriction is the tendency for bonded stringers to separate from the skin once buckling occurs. If this design restriction can be modified to allow local buckling at design limit load, as long as the structure does not fail at load less than design ultimate load, lighter, more weight- and cost-efficient structures can be realized.

*Senior Aerospace Engineer, Structural Mechanics and Concepts Branch. Associate Fellow, AIAA.
**Principle Design Engineer, Advanced Structures R&D, Senior Member, AIAA.
+Engineering Manager, Advanced Manufacturing and Structures Technology Group.

Panels can be designed such that the panel is assumed to carry load and remain intact for loads significantly greater than the buckling load. The primary objective of the proposed study is to evaluate the potential weight savings of allowing stiffened panels to buckle at load less than the ultimate load as long as the panel does not fail. If specimen failure load is considered to be the ultimate load, local damage initiation and growth and nonlinear post-buckling behavior must be considered. The approach taken in this paper is to study the behavior of single-stiffener specimens both experimentally and analytically, and utilize this knowledge to infer the structural efficiency gains for multi-stiffener panels through analytical studies.

While a blade-stiffener is structurally efficient, the addition of unidirectional fibers at the top of a thin blade provides more stiffness (per unit weight) and could lead to more structurally efficient designs. The concept of integral stiffeners with a concentration of material in a "bulb" on a thin web is discussed in terms of load-carrying ability, structural efficiency and buckling behavior in reference 4 for aluminum and titanium panels for aircraft applications. The idea of carbon-rod stiffeners has been examined in several studies.[5-7] Researchers have been developing the concept of "rods" added to the top of a thin blade and wrapped with a layer of angle ply. A study of the behavior of blade-stiffened crippling specimens is presented in reference 8 and some of those are results are presented herein. The goal of this study is to examine the behavior of rod-stiffened structures and compare these results to the earlier blade-stiffener results.

II. Test Specimen Description

Blade-stiffened and rod-stiffened specimens were fabricated from stitched/resin infused graphite-epoxy material. The details of the geometry and manufacture of blade-stiffened specimens are presented in reference 8 to 10 so limited descriptions are presented herein. The manufacturing process for the rod-stiffened specimens is presented in reference 11. In both cases, skin and stiffeners are composed of layers of graphite material forms that were prekitted in nine-ply stacks using Hercules, Inc. AS4 fibers. Each nine-ply stack had a $[45/-45/0_2/90/0_2/-45/45]_T$ laminate stacking sequence. Stack thickness was approximately 0.055 inches for the blade-stiffened specimens and 0.052 inches for the rod-stiffened specimens. Several stacks of the prekitted material were used to build up the desired thickness and configuration. Blade-stiffened specimens were stitched together using E. I. DuPont de Nemours, Inc. Kevlar thread while rod-stiffened specimens were stitched together using Vectran fibers. Stiffener flanges were stitched to the skin and no mechanical fasteners were used for joining. The blade-stiffened specimens were fabricated using Hercules, Inc. 3501-6 epoxy in a resin infusion process which is described in references 9 and 10 while the rod-stiffened specimens are made from HexFlow VRM 34 resin, as described in ref. 11. Unidirectional carbon fiber rods at the top of the web and angle-ply AS4 carbon fiber overwraps around the rods were used for the rod-stiffened specimens. Material properties for a stack of material in each system are shown in table 1.[12,13] These properties were determined from fabricated stacks, and therefore already take into account the influence of the stitches on the in-plane properties.

Table 1. Material stack properties

Property	Blade-stiffened	Rod-stiffened
Longitudinal stiffness, Msi	9.27	9.74
Transverse stiffness, Msi	4.67	4.87
Shear stiffness, Msi	2.27	2.57
Major Poisson's ratio	0.397	.400
Stack thickness, in.	0.055	.052
Allowable compressive strain, in./in.	-0.0089	NA
Allowable tensile strain, in./in.	0.0121	NA
Ultimate stress, compressive, ksi	NA	-82
Ultimate stress, tensile, ksi	NA	112
Rod stiffness, Msi	NA	19.09
Rod cross sectional area, in^2	NA	0.1802
Density, lb/in^3	0.057	.057

As mentioned in the introduction, results for a blade crippling specimen that was studied in reference 8 is presented herein to provide a comparison with the present rod-stiffened specimen results. In order to evaluate response and failure of the blade-stiffened design, a crippling specimen was fabricated "back-to-back" resulting in two stiffeners jointed together in an X shape.[8] This configuration resulted in a double thickness flange. Rod-stiffened specimens were not fabricated in this manner. Sketches of the cross section of a blade- and rod-stiffened specimens are shown in fig. 1 and photographs of typical specimens are shown in fig. 2. Blade specimens had a 5.0-inch wide flange, a 0.11-inch thick blade, and a 3.0-inch tall stiffener. Rod-stiffened specimens had a 3.4-inch wide flange, a 0.104-inch thick stiffener web and a 1.5-inch tall stiffener. Flange thickness was half the blade or web thickness, Blade- and rod-stiffened specimens were 12 and 18 inches tall, respectively. Blade-stiffened-specimens were fabricated in an autoclave while rod-stiffened specimens were fabricated in an out-of-autoclave process. In each case, the entire

perform was stitched together prior to curing. In addition to the stitched rod-stiffened specimens, one specimen with the same geometry and materials as the rod-stiffened specimens was fabricated with no stitching. Prior to testing, each end of the specimen was potted in 1.0-inch-deep epoxy compound and the ends were ground flat and parallel to each other to ensure uniform load introduction.

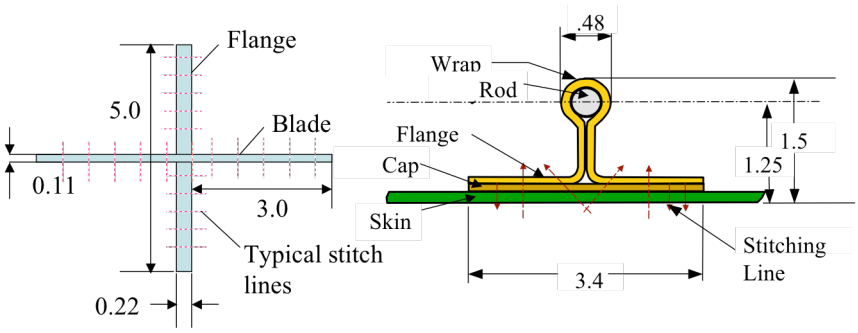

a) Blade-stiffened specimen. b) Rod-stiffened specimen.

Figure 1. Test specimen geometry. All dimensions are in inches.

III. Test Procedure and Instrumentation

Three rod-stiffened specimens with identical geometry were loaded in the same manner as the blade-stiffened specimens in the previous study.[8] All specimens were loaded to failure in axial compression. Load rates varied among the different tests, but generally tests were planned to run for 15-30 minutes. Displacement and strain gage data were recorded at the rate of once every second as load was applied during each test. Buckling and failure behavior were noted for each specimen.

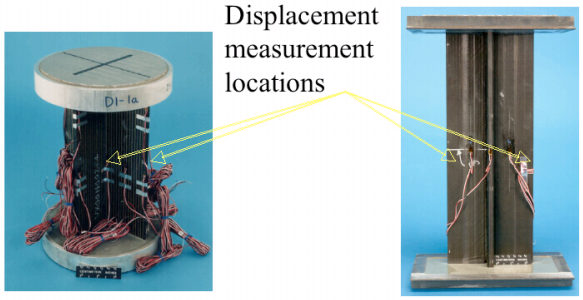

a) Blade-stiffened specimen b) Rod-stiffened specimen

Figure 2. Strain gage and displacement measurement locations.

Displacements were measured using two displacement transducers measuring end-shortening, and two measuring out-of-plane displacement at the midlength location. Out-of-plane measurement locations were at the edge of the flange and blade for the blade-stiffened specimens and at the specimen edges for the rod-stiffened specimens. Twenty-four back-to-back strain gages were used to monitor strains in the flanges and blades of the blade-stiffened specimens and six back-to-back strain gages were used on the skin and rod region of the rod-stiffened specimens. Strain gages were located midlenegth on both specimens. Typical strain gage and displacement measurement locations are shown in fig. 2. An optical measurement system[14] was used to obtain full field displacement and strain results for the unstiffened side of the skin or the rod-stiffened specimen as well.

IV. Finite Element Analysis

The blade- and rod-stiffened specimens were analyzed using the STAGS[15] finite element computer code. The analysis accounts for geometric nonlinearities but not plasticity. All structural components are modeled using quadrilateral shell elements except the rods which were modeled as beam elements attached to the top of the stiffener webs. The through-the-thickness stitches are not modeled in the analysis because previous studies[1,16] have shown that good results can be obtained without modeling the stitches. The buckling loads and mode shapes, the post-buckling behavior, and the damage initiation and growth are studied using the same approach utilized in reference 8.

The finite element model for a blade-stiffened specimen is shown in fig. 3a and has 7,820 nodes and 7,644 elements, for a total of 46,920 degrees of freedom. The finite element model for a rod-stiffened specimen is shown in fig. 3b and has 5,661 nodes and 4932 elements, for a total of 34,948 degrees of freedom. All degrees of

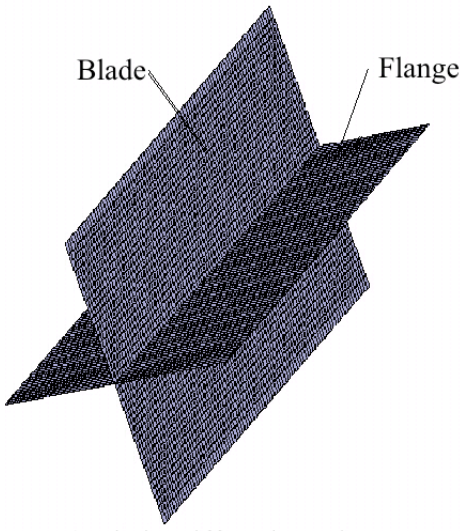

a) Blade-stiffened specimen

Figure 3. Finite element models.

freedom on one end of the specimen were restrained. For a region of one inch from each end, i.e., inside the potted region, all degrees of freedom were restrained except for the shortening of the specimen. A load was applied on one end of the specimen and all nodes on that end were constrained to move the same amount. The potting material was not modeled.

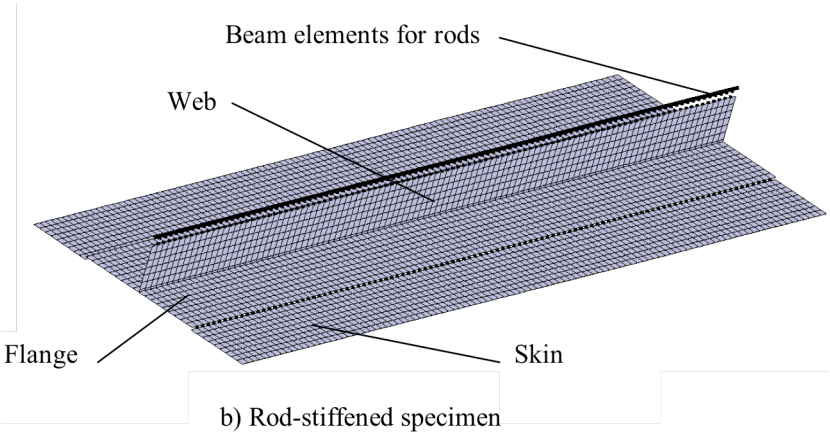

b) Rod-stiffened specimen

Figure 3. Concluded.

Each configuration was first analyzed to determine the linear, nonlinear and buckling behavior using assumed properties for each stack of material not individual ply properties. Buckling loads were calculated based on a linear prebuckling stress state. Then a nonlinear analysis was conducted and buckling mode shapes were calculated based on the nonlinear stress state at a load within 10 percent of the linear prediction of the buckling load. Then an assumed initial imperfection in the shape of the buckling mode corresponding to the minimum buckling load was input. An imperfection mode with an amplitude of 0.001 inches (approximately 1/100 of the thinnest skin) was input to trigger nonlinear behavior for loads equal to and greater than the buckling load.

The damage initiation and growth was then analyzed using the approach described in references 8 and 14. The progressive failure analysis was conducted using the STAGS finite element code to determine the load at which the first element would sustain damage. Properties for each ply in each stack were used in the failure analysis. The additional input required for using this technique is described in reference 15. Results obtained using a similar method are presented in references 16 and 17 and illustrate the failure prediction capability of this method. Ply properties used for the blade-stiffened specimens are the same as those used in reference 8 and are given in table 2. Less stitching in the skin and improvements in manufacturing led to in-plane stack stiffness properties for the rod-stiffened specimens which are greater than for the blade-stiffened specimens. Since the stacking sequence of a stack of material is the same for the blade- and rod-stiffened specimens and ply properties for the newer stitched material with the Vectran reinforcement and improved resin were unavailable, the ply properties used for the rod-stiffened specimen analysis were determined by scaling the blade-stiffened ply properties such that the A matrix of plies corresponding to a stack of material was the same as the A matrix of the measured rod-specimen stack. Ply failure strains for rod-stiffened specimens are determined from stack stiffness and stack failure stress, so each ply is assumed to have the same failure strength. Assumed ply properties for the rod-stiffened specimens are given in table 2. This failure prediction method evaluates the strains and stresses in all plies in all elements and compares these values to the defined failure values (as shown in table 2 for each ply). As the failure values are exceeded,

Table 2. Nominal ply properties.

Property	Blade stiffened			Rod- stiffened		
	0^o	$+45^o$ and -45^o	90^o	0^o	$+45^o$ and -45^o	90^o
Longitudinal stiffness, Msi	16.43	16.15	15.97	17.42	17.12	16.93
Transverse stiffness, Msi	1.60	1.60	1.60	1.70	1.70	1.70
Shear stiffness, Msi	0.80	0.80	0.80	0.80	0.80	0.80
Major Poisson's ratio	0.34	0.34	0.34	0.34	0.34	0.34
Ply thickness, in.	0.0061	0.0061	0.0061	0.0058	0.0058	0.0058
Failure compressive longitudinal strain, in/in.	-.0104	-.0104	-.0104	-.0082	-.0082	-.0082
Failure tensile longitudinal strain, in/in.	.0128	.0128	.0128	.0115	.0115	.0115
Failure compressive transverse strain, in/in.	-.0104	-.0104	-.0104	-.0082	-.0082	-.0082
Failure tensile transverse strain, in/in.	.00955	.00955	.00955	.0115	.0115	.0115
Failure shear strain, in/in.	.02	.02	.02	.02	.02	.02

appropriate ply level material properties are degraded and the ply loses its ability to carry load as the load to the structure is increased. Analytical results are obtained by examining the amount of damage and the location of damaged elements within the specimen at each load step. Each element in a model contains numerous locations where the stress and strain are calculated. The amount of damage in an element is expressed in terms of the percentage of these points which have strains in excess of the input failure value as described in reference 15.

V. Results and Discussion

Results for three configurations of blade-stiffened specimens are presented in reference 8 but only the results for the specimens with a two-stack skin and two-stack blade are presented herein. Results for rod-stiffened specimens are presented also presented in this section. Analytical and experimental results for blade- and rod-stiffened single-stiffener specimen and analytical predictions of stiffened panels are presented in this section. Analytical results are represented by solid lines and experimental results are represented by dashed lines. A summary of the single-stiffener and panel results are shown in tables 3 and 4, respectively.

Table 3. Behavior of single-stiffener specimens

	Blade-stiffened	Rod-stiffened, stitched	Rod-stiffened, unstitched
Buckling, experimental, kips	20	22	22
Buckling, analysis, kips	20	22	NA
Failure, experiment (kips)	71	45,46*	46
Initial damage, analysis (kips)	30	38	NA
Failure, analysis (kips)	55	41	NA
Ratio of damage load to buckling load (analysis)	1.5	1.8	NA
Ratio of failure load to buckling load (analysis)	2.7	1.9	NA

*Two specimens were tested

A. Displacements and Buckling Loads

Experimental and analytical results for end-shortening and out-of-plane deformation are shown in figures 4 and 5 for blade-and rod-stiffened specimens, respectively. Experimental and analytical results agree well in each case. Buckling mode shapes from finite element analysis for blade-and rod-stiffened specimens are shown in figures 6 and 7, respectively. Calculated and experimentally determined buckling loads are presented in table 3. Analytical results indicate that no failures occur prior to buckling.

Table 4. Behavior of multi-stiffener specimens*

Configuration	Blade	Blade	Blade	Rod
Blade/web thickness (in.)	0.11	0.22	0.33	0.104
Flange thickness (in.)	0.055	0.11	0.22	0.052
Skin thickness (in.)	0.11	0.11	0.11	0.104
Bucking load (lb)	38,588	128,888	262,303	57,380
Critical running load (lb/in.)	1,837	6,137	12,490	2,732
Failure load based on single-stiffener specimen (lb)	100,328	166,083	284,786	107,347

*Panels were 21 inches long with 7-inch stiffener spacing

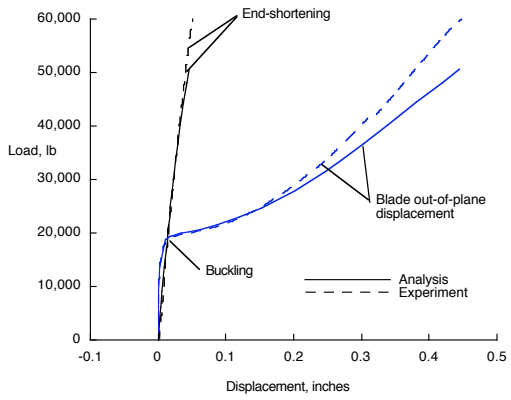

Figure 4. Measured and predicted displacements for blade-stiffened specimen.

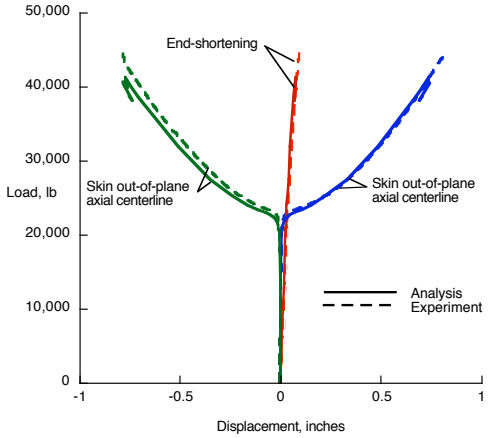

Figure. 5. Measured and predicted displacements for rod-stiffened specimen.

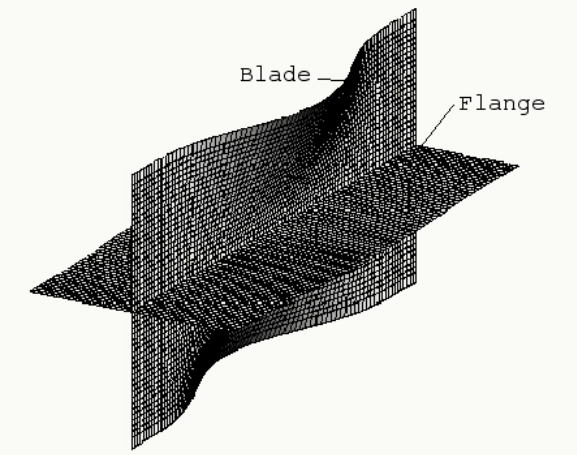

Figure 6. Buckling mode shape for blade-stiffened specimen.

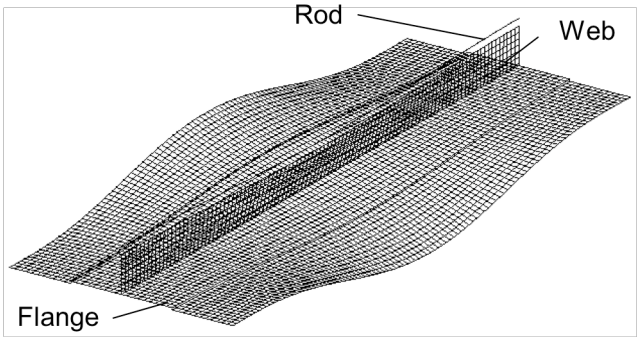

Figure 7. Buckling mode shape for rod-stiffened specimen.

B. Strain

The blade-stiffened specimen was loaded to 60,000 lb, unloaded and then loaded to failure. Experimental and analytical strains at the midlength location of the blade at its tip for are shown in fig. 8. There is excellent agreement between strain gage results and experimental predictions, indicating the accuracy of the predicted buckling load of 20,000 lb. The axial strains throughout the specimen as determined from finite element analysis are shown in fig. 9. The axial strains at an applied load of 72,000 lb, range from an axial compressive strain of -0.015 in./in. to a tensile strain of 0.0085 in./in. The value of 72,000 lb corresponds approximately to the experimental failure load of the specimen. These analyses were geometrically nonlinear, but used smeared stack properties and no progressive failure was simulated. Since the allowable compressive strain of this material is -0.0089 in./in. this compressive strain represents more than 15% greater than the allowable and failure would be expected.

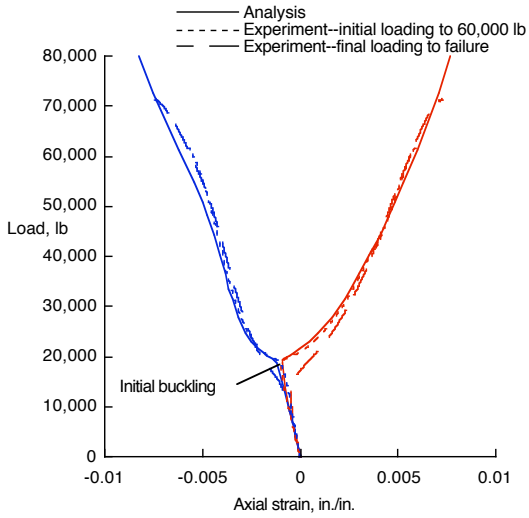

Figure 8. Measured and predicted strain midlength in blade-stiffened specimen.

Using the individual ply properties rather than stack properties in the progressive failure analysis allows for a more detailed prediction of failure. The buckling load was unaffected by the change in properties. The progressive failure analysis of a blade-stiffened specimen indicates that no damage would occur for load less than 30,000 lb, or 1.5 times the buckling load. Damage initiates in the blade mid-length, where the blade joins the flange. Damage progresses to include the center of the blade and then the corners at the edge of the potted region of the flange. Damaged regions at an applied load of 2.7 times the buckling load are shown in fig. 10. The shades in fig. 10 represent the amount of damage in each element. Each element in the model contains numerous locations where the stress and strain are calculated. The amount of damage in an

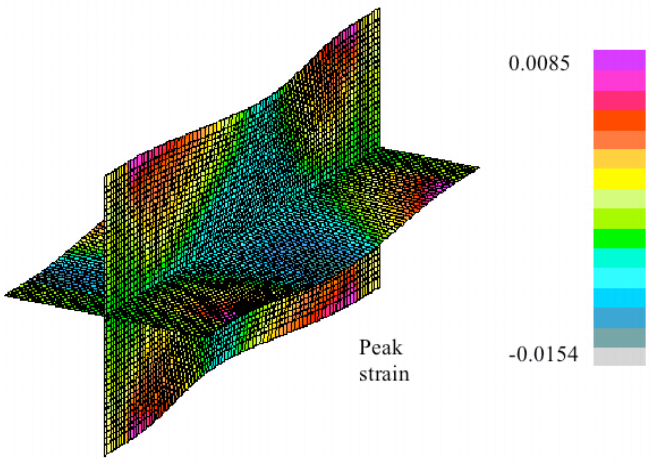

Figure 9. Axial surface strain contours for blade-stiffened specimen at an applied load of 72,000 lb.

element is expressed in terms of the percentage of these points which have stresses in excess of the input failure value. No element is more then 25 percent failed at an applied load of 2.7 times the buckling load.

Primary failure of the test specimen is along the axial centerline in the blade and flange. In addition, the bond between the two flange pieces at the edge failed, as shown in fig. 11. The finite element analysis assumes a perfect bond and has no means to evaluate through-the-thickness failures. The failure load, however, is more than three times the buckling load. After the blades buckle, the load is concentrated in the flange and at the intersection of the flange and blade. Therefore, it is to be expected that the specimen would fail at these locations.

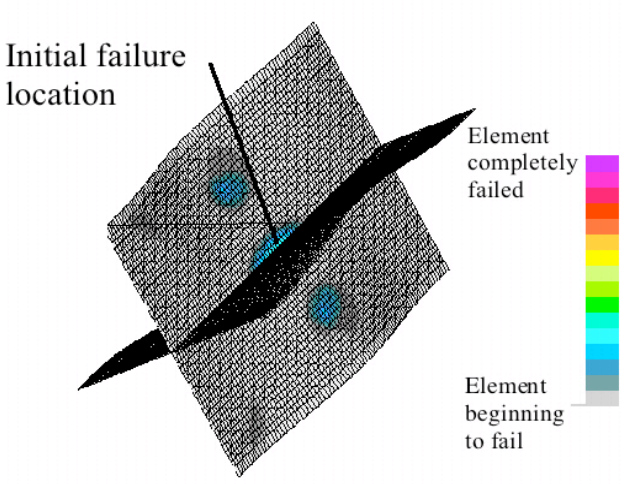

Figure 10. Damaged elements for an applied load of 2.7 times the buckling load for blade-stiffened specimens

Experimental and analytical strains at the midlength location of skin for the rod-stiffened specimen are shown in fig. 12. There is good agreement between strain gage results and experimental predictions verifying the accuracy of the predicted buckling load of approximately 22,000 kips. The axial strains throughout the specimen as determined from finite element analysis are shown in fig. 13. The axial strains at an applied load of 38,831 lb range from an axial compressive strain of -0.005 in./in. to a tensile strain of 0.0091 in./in. The value of 38,831 lb corresponds to approximately 95% of the experimental failure load of the specimen.

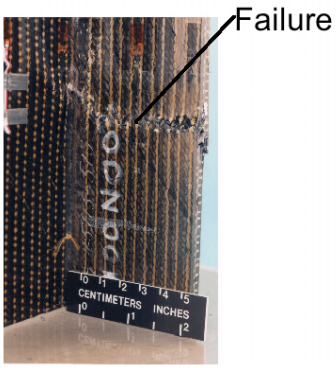

Figure 11. Failed blade-stiffened specimen.

Using the individual ply properties in the progressive failure analysis results in a predicted buckling load decrease from 22,451 lb to 21,394 lb due to the change in properties. The progressive failure analysis of a rod-stiffened specimen indicates that no damage would occur for load less than 38,000 lb, or 1.8 times the buckling load. Damage initiates in the stiffener web mid-length. Damaged regions at an applied load of 1.9 times the buckling load are shown in fig. 14. The shades in figure 14 represent the amount of damage in each element. No element is more then 25 percent failed at an applied load of 1.9 times the buckling load, however continuing the analysis past this point does not results in a higher load, only more element failures and greater displacements, indicating a maximum load has been attained, i.e. specimen failure at approximately 40,600 lb.

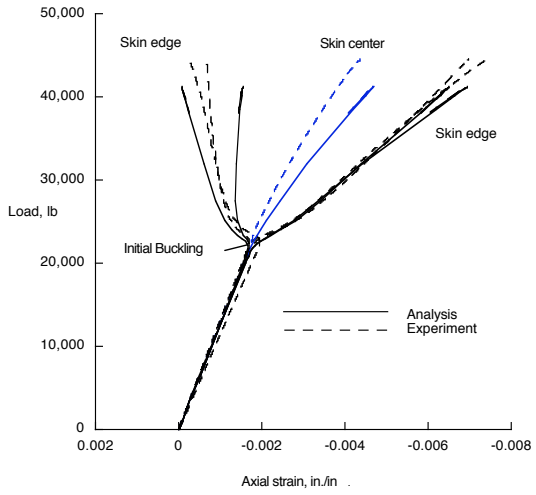

Figure 12. Measured and predicted strains midlength in skin of rod-stiffened specimen.

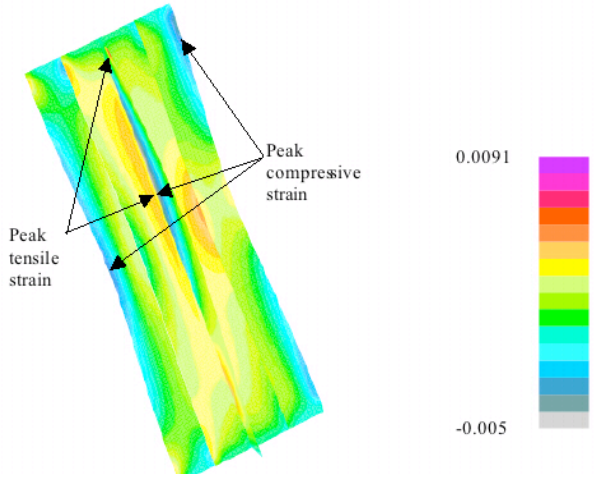

Figure 13. Axial surface strain contours for rod-stiffened specimen at an applied load of 38,831 lb.

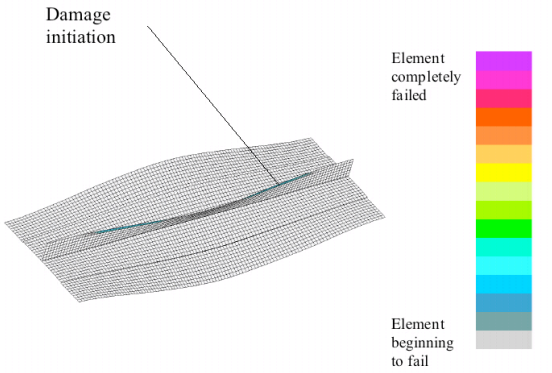

Figure 14. Damaged elements for an applied load of 1.8 times the buckling load for a rod-stiffened specimen.

One specimen with rod-stiffening was fabricated without skin-to-flange stitches to determine the value of these stitches. A plot of the measured displacements of stitched and unstitched rod-stiffened specimens is shown in fig. 15 showing that the stitches have no noticeable effect on the buckling or failure load of these specimens. However, the photographs of failed specimens shown in figures 16 and 17 show that the failure mode of the stitched and unstitched specimens are different. The flange and skin separate over a much longer region for the unstitched skin than in the stitched skin. The stitching suppresses a delamination between the flange and skin after the specimen buckles that can be seen in the failed unstitched specimen. In addition to suppressing delamination in pristine region such as seen here, stitches would reduce or prevent delamination in an impact damaged specimen, improving the damage tolerance of this configuration.[18]

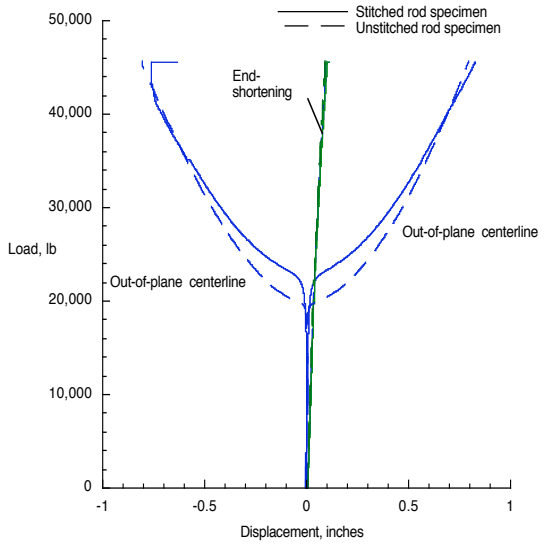

Figure 15. Measured displacements at midlength of stitched and unstitched rod-stiffened specimens.

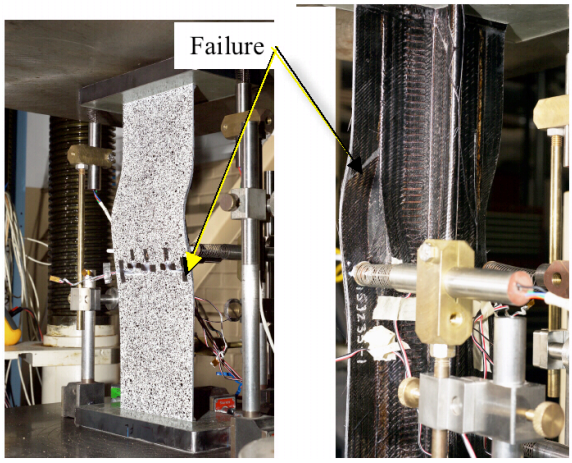

Figure 16. Failure of stitched rod-stiffened specimen.

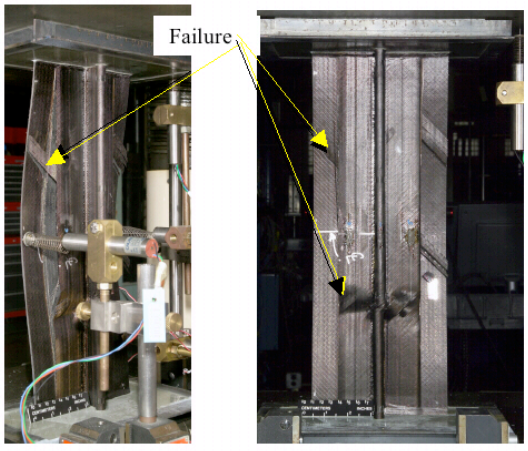

Figure 17. Failure of unstitched rod-stiffened specimen.

C. Structural Efficiency of Stiffened Panels

Structural efficiency is expressed in terms of weight versus load carrying capability. In the past, these values would be based on global or local buckling with no load carrying capability considered for loads greater than the buckling load. However, since the purpose of this study is to evaluate the potential weight savings of allowing panels to buckle prior to ultimate load, buckling is not considered to be the maximum allowable load. A maximum strain failure criterion is used such that strains may not exceed the allowable strains presented in table 1. To eliminate the effects of length, efficiency is expressed herein as weight/(planform area * length) (W/AL) vs. running load /length (N_x/L), as discussed in reference 2. Using this format, a lower a specimen weight ratio for a given load ratio and conversely, a higher the load ratio for a given weight ratio,

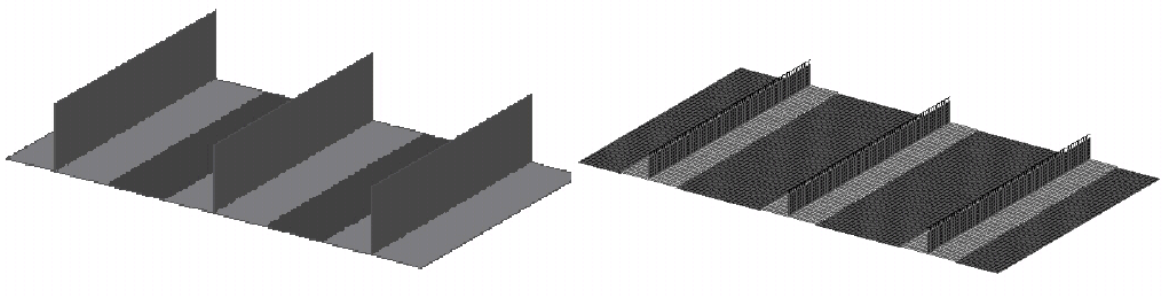

Figure 18. Stiffened panel configuration. Dimensions are shown in table 4.

indicates a more structurally efficient design. Values are shown based on three assumptions: 1) no buckling is permitted at loads less than ultimate load, 2) buckling is permitted for loads greater than design limit load only, and 3) buckling is permitted at any load and ultimate load is determined by other means. Obviously, the last of these options may produce the most efficient structure, but it may be impractical for aerodynamic or other reasons to allow buckling at less than design limit load.

Results included herein include all configurations of specimens presented in ref. 8 that buckled prior to failure and the rod-stiffened configuration. The geometry of blade- and rod-stiffened configurations was extrapolated to a 21-inch-wide panel with a 7-inch stiffener spacing. Blade and rod dimensions were left unchanged but skin regions (without flanges) were assumed to be 3-inches wide. All panels were assumed to be 12-inches long and held between clamped loaded edges. Unloaded edges were assumed to be free. Skin thickness is 0.11-inches for blade-stiffened panels and 0.104 for rod-stiffened panels. Sketches of the panel configurations are shown in fig. 18 and the skin, blade and flange thicknesses for the panels considered are shown in table 4.

Structural efficiency results are based on buckling loads from finite element analysis of the panels and damage progression assumed to match the damage progression of the corresponding single-stiffener specimen. The buckling load for the panel with blade-stiffened panel with a 2-stack skin and 2-stack blade is 38,588 lb, or 1,837 lb/in. across the 21 inch width. If the panel behaves the same way as the single-stringer panel, the panel would fail at 2.7 times the buckling load, or 100,328 lb. Similarly, the buckling load of the rod-stiffened panel is 57,380 lb or 2,732 lb/in across the width. By assuming the panel fails at a load of 1.9 times the buckling load, as for the single stiffener specimen, a panel failure load of 107,347 lb is obtained. Critical loads are shown for panels corresponding to all panel configurations examined in reference 8 and rod-stiffened panels are shown in table 4.

Structural efficiencies based on the assumption that ultimate load is the buckling load (shown as open bars) and that the ultimate load is 1.5 times the buckling load (shown as shaded bars) are shown in fig. 19. Also shown in the figure are predictions assuming the ultimate load is the load at the first damage event (based on the load of the first damage event predicted for the single-stiffener specimen and shown as cross-hatched bars) and assuming that the ultimate load is the load when 5% or more of the elements are damaged (shown as filled bars). For the 2-stack blade specimen, the first damage event occurs at 1.5 times the buckling load but damage does not progress to encompass 5% of the elements until 2.7 times the buckling load. An increase in load of 50% can be achieved by allowing the panel to buckle at limit load rather than at ultimate load. The rod-stiffened panel weighs 17% more than this blade-stiffened panel but it carries 48% more load at buckling. In addition, first failure in the rod-stiffened panel is at 78% greater load than the blade-stiffened panel. However, the failure load is only 10% greater in the rod-stiffened panel than in the blade-stiffened panel. Displacement patterns for blade-

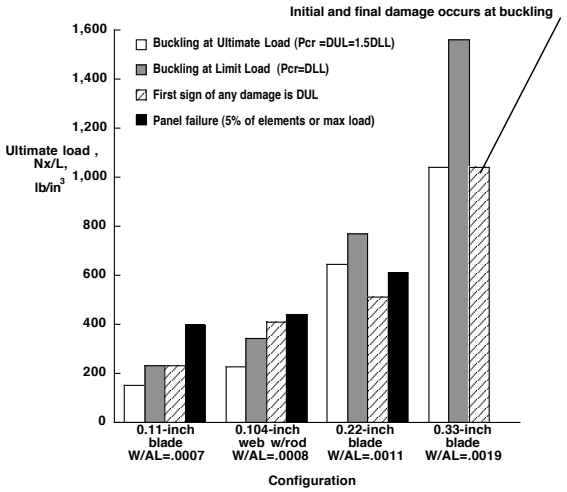

Figure 19. Structural efficiency of stiffened panels.

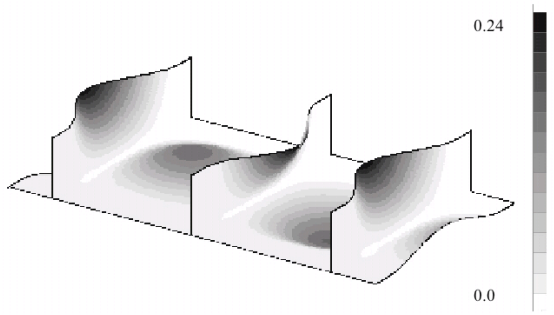

Figure 20. Deformation pattern for blade-stiffened panels at a load of 1.5 times the buckling load. Dimensions are in inches.

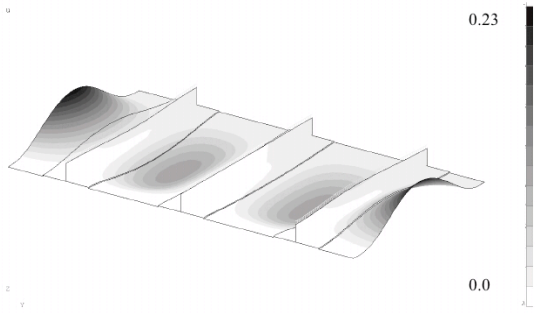

Figure 21. Deformation pattern for rod-stiffened panels at a load of 1.5 times the buckling load. Dimensions are in inches.

and rod-stiffened panels at a load of 1.5 times the buckling load are shown in figures 20 and 21, respectively. The blade-stiffened specimen buckles in the skin and in the stiffener while the rod-stiffened specimen buckles only in the skin. Strain contours for blade- and rod-stiffened panels at a load of 1.5 times the buckling load are shown in figures 22 and 23, respectively. Strains at 1.5 times the buckling load are significantly less than failure strains. The rod-stiffened panel is more structurally efficient than the blade-stiffened panel because more material is positioned further away from the center of cross section in this configuration.

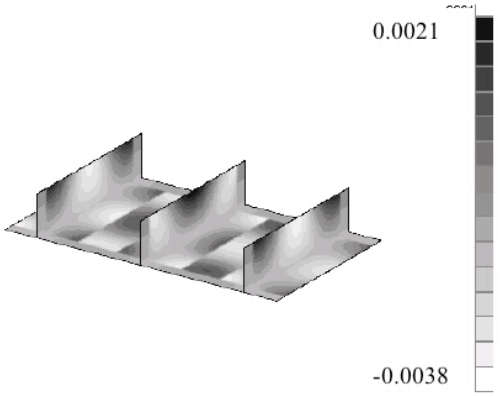

Figure 22. Axial strain for blade-stiffened panel at an applied load of 1.5 times the buckling load. Strains are in in./in.

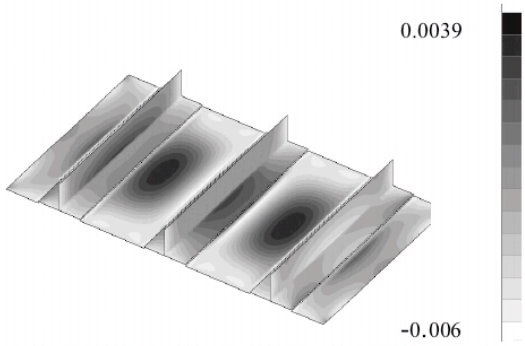

Figure 23. Axial strain for rod-stiffened panel at an applied load of 1.5 times the buckling load. Strains are in in./in.

VI. Concluding Remarks

The structural efficiency of rod-and blade-stiffened stitched specimens is compared to determine their weight saving potential if stiffeners of composite aircraft components were allowed to buckle at loads less than design ultimate load. Blade- and rod-stiffened specimens were examined experimentally and by using finite element analysis. Analytical and experimental results are in good agreement. Buckling and strain results indicate that thin-skin and thin-blade configurations demonstrate significant potential weight-savings by allowing a post-buckled design. Rod-stiffened specimens are more structurally efficient than blade-stiffened specimens by increasing buckling loads by almost 50%. The lightly loaded specimen configuration would be useful in less stressed wing sections, such as near the wing tip, where a stiffener and/or skin could be allowed to buckle at load as low as design limit load without failure to any part of the wing. In addition stitching the flange to the skin changes the failure mechanism by suppressing delamination between the flange and skin.

Acknowledgments

The authors wish to thank Steve Clay and Dick Holzwarth of the Air Force Research laboratory for their support of this technology.

References

[1]Karal, M, "AST Composite Wing Program - Executive Summary," NASA CR 2001-210650, August 2001.

[2]Williams, J., Anderson, M., Rhodes, M., Starnes, J., and Stroud, J., "Recent Developments in the Design, Testing and Impact-Damage Tolerance of Stiffened Composite Panels." NASA TM 80077.

[3]Jegley, D., "Study of Compression-Loaded and Impact Damaged Structurally Efficient Graphite-Thermoplastic Trapezoidal-Corrugation Sandwich and Semisandwich Panels," NASA TP 3264, Nov. 1992.

[4]McQueen, J.C., McClaren, S.W. and Martin, A. P., "Integrally Formed Structures: A New Stiffened Panel Concept," *Journal of Aircraft*, Vol. 7, No. 6, Nov.-Dec. 1970.

[5]Baker, Donald J., and Rousseau, Carl Q., "Evaluation of Carbon-Rod Reinforced Crippling Strength Specimens," Presented at the AIAA/ASME/ASCE/AHS/ASC 40th Structures, Structural Dynamics, and Materials Conference, St. Louis, MO, AIAA Paper 99-1282, April 12-15, 1999.

[6]Rousseau, Carl Q , Baker, Donald J., Chan, and Wen S., "Analysis and Testing of Graphite Rod-Reinforced Hat-Section Stringer," Presented at the AIAA/ASME/ASCE/AHS/ASC 36th Structures, Structural Dynamics, and Materials Conference, New Orleans, LA, AIAA Paper 95-1509, April 10-12, 1995.

[7]Baker, Donald J., and Rousseau, Carl Q., "Analysis and Test of Repair concepts for a Carbon-Rod Reinfored Laminate," Presented at the AIAA/ASME/ASCE/AHS/ASC 41st Structures, Structural Dynamics, and Materials Conference, Paper 2000-1596, April 2000.

[8]Jegley, Dawn C., "Structural Efficiency Of Stitched Composite Panels With Stiffener Crippling," *Journal of Aircraft*, Vol. 42, No. 5, pp. 1273-1280, September-October, 2005.

[9]Markus, A., Thrash, P., and Grossheim, B., "Manufacturing Development and Requirements for Stitched/RTM Wing Structure," NASA CP 3229, 1993, pp. 503-523.

[10]Rohwer, K., Ghumman, A., and Markus, A., "Stitched/Resin Film Infusion (S/RFI) Manufacturing Technology Development," Proceedings of the 11th DOD/NASA/FAA Conference on Fibrous Composites in Structural Design. Report number WL-TR-97-3009 pp. XIII-93-116.

[11]Velicki,A. and , Thrask, P., "Advanced Structural Concept Development Using Stitched composites," AIAA/ASME/ASCE/AHS/ASC 49th Structures, Dynamics and Materials Conference, Schaumburg, IL, April 2008.

[12]Hinrichs, S., "General Methods for Determinig Stitched composite Material Stiffnesses and Allowale Strenghts, Vol I," McDonnell Douglas Rept. MDC94K9113, Long Beach CA, March 1995.

[13]"Warp/knit Multi-Axial Carbon Fiber Fabric," The Boeing Co. Report, DMS 2436H, Long Beach CA, 2005.

[14]Davila, C. G., Ambur, D. R., and McGowan, M., "Analytical Prediction of Damage Growth in Notched Composite Panels Loaded in Axial Compression," *Journal of Aircraft*, Vol. 37, No. 5, Sept-Oct. 2000.

[15]Rankin, C. C., Brogan, F. A, Loden, W. A., and Cabiness, H. D., "STAGS User Manual, Version 4.0." Lockheed Martin Missiles and Space Company, Incorporated, Palo Alto, CA, May 2001.

[16]McGowan, D. M., Davila, C. G., and Ambur, D. R., "Damage Progression in Buckle-Resistant Notched Composite Plates Loaded in Uniaxial Compression," AIAA Paper 01-1482, Apr. 2001.

[17]Sleight, D.W., Knight, N. F., Wang, J. T., "Evaluation of a Progressive Failure Analysis Methodology for Laminated Composite Structures," AIAA Paper 97-1187, Apr. 1997.

[18]Jegley, D. C. "Improving Strength of Postbuckled Panels Through Stitching," *Composite Structures*, Vol. 80, 2006, pp. 298-306.